Disordered FPUT-α Hamiltonian Lattices: recurrence breakdown and chaotic behavior

Disordered FPUT-α Hamiltonian Lattices: recurrence breakdown and chaotic behavior

Zulkarnain[a,b], H. Susanto[c,*], C. G. Antonopoulos[a]

[a] *School of Mathematics, Statistics and Actuarial Science, University of Essex, Wivenhoe Park, Colchester, CO4 3SQ, United Kingdom*
[b] *Department of Mathematics, Universitas Riau, Pekanbaru, 28293, Indonesia*
[c] *Department of Mathematics, Khalifa University, Abu Dhabi, PO Box 127788, United Arab Emirates*

Abstract

This paper studies a modified Fermi-Pasta-Ulam-Tsingou (FPUT)-α Hamiltonian lattice, where variability is introduced to the system through the potential parameters. By a transformation, the system is equivalent to the FPUT-α lattice with random masses. We fix the energy level and investigate how energy recurrences disappear as the percentage of variability increases from zero. We observe that the disappearance of energy recurrences leads to either localization or thermalization of normal-mode energy. When energy localization occurs, we derive a two-mode system by using multiple-scale expansions to explain the route to localization as the percentage of variability increases. Furthermore, we investigate the chaotic behavior of the system by computing the maximum Lyapunov exponent for different percentages of variability. Our results show that the number of particles increases the chances of observing chaotic dynamics for small percentages of variability. Meanwhile, the effect reverses as the percentage of variability introduced to the system rises from zero.

Keywords: FPUT-α Hamiltonian, FPUT energy recurrences, variabilities, chaos, Lyapunov exponents
2010 MSC: 00-01, 99-00

1. Introduction

Fermi, Pasta, and Ulam conducted numerical simulations in 1953 with Tsingou's assistance. They investigated the rate of approach to energy equipartition in a dynamical system describing a one-dimensional particle chain with nonlinear forces between particles, known as the FPUT lattice with fixed ends [1]. They expected that quadratic forces would allow continuous energy transfer from the initially excited first normal mode to higher-order normal modes, leading to energy thermalization or mixing. Instead, energy exchange occurred only among a few modes before returning down within one percent of its initial value, so the system appeared nearly periodic. This recurrence phenomenon was confirmed over a longer period of time following the work in [2, 3],

*Corresponding author
Email address: hadi.susanto@yandex.com (H. Susanto)

where authors also observed the appearance of super recurrence, in which more energy returned to the initially excited mode.

Nelson et al. [4] introduced disorder into the FPUT system in several different ways to study its effect on energy recurrences. They observed that it can destroy energy recurrence and increase thermalization as the percentage of variability in the system's parameters increases. The effect of disorder on the thermalization of lattice systems is usually studied through randomly varying particle masses. Considerably, the first study in disordered *harmonic* lattices was due to Allen and Ford [5] who observed a finite thermal conductivity in the system, unlike the concept of Anderson localization [6] in which the conductivity will exponentially decay to zero. This is because of the delocalized low-frequency phonons [7], that prevents the disordered harmonic lattices from being a thermal insulator. Li et al. [8] conducted the first systematic study of the mass disorder effect in anharmonic (FPUT) lattices connected to heat baths, followed by the work of, e.g., Dhar and Saito [9] and Zhu et al. [10] on finding the correct conductivity exponent (see also Liu et al. [11] for a review on the topic).

In this work, we are interested in investigating the localization of normal-mode energy for a disordered FPUT-α system with fixed ends at a fixed energy level. The disorder is introduced into the system through the heterogeneity of the potential parameters and controlled by a variability percentage. We show by a transformation that the system under consideration is equivalent to the FPUT with mass disorders. We employ the same constant energy as in the initial FPUT experiment, where the recurrence phenomenon was observed. Due to the disorder, we show that the recurrence breaks down, which leads to energy localization. To explain the localization mechanism, we work in normal-mode space to establish a two-mode approximation for the FPUT-α system. Following the works in [12, 13], this two-mode system can be interpreted as a two-frequency solution on q-tori.

The remainder of this paper is structured as follows: Section 2 examines the original FPUT lattice with quadratic nonlinearity (i.e., the FPUT-α system) and discusses energy recurrences. We introduce the disordered FPUT-α system in Section 3. The phenomena of energy recurrence breakdown are discussed in the same section. Using multiple-scale analysis, we derive a two normal-mode approximation in normal-mode space in Section 4. Our analytical results explain why energy recurrences fail when variability is introduced. Section 5 discusses chaos in the FPUT-α system with or without variability by computing the maximum Lyapunov Exponent (mLE) to distinguish between regular and chaotic dynamics. Finally, we conclude our study in Section 6.

2. Mathematical model and dynamics of FPUT-α lattices

The FPUT-α lattice is a one-dimensional chain of particles connected by nonlinear forces acting on adjacent particles. If $x_j(t)$ denotes the shift of the j-th particle from its equilibrium position as a function of time t and $p_j(t)$ is its associated conjugate momentum as a function of time t, then the Hamiltonian of the system is given by

$$H(x,p) = \sum_{j=0}^{N} \frac{1}{2} p_j^2 + \sum_{j=0}^{N} \frac{1}{2} \left(x_{j+1} - x_j\right)^2 + \frac{\alpha}{3} \left(x_{j+1} - x_j\right)^3 = E, \tag{1}$$

where fixed boundary conditions (fixed ends) $x_0 = x_{N+1} = 0$ have been used. Here, E is the total, fixed energy of the system, while $\alpha \geq 0$ is the nonlinearity strength. Therefore, the equations of motion are given by

$$\ddot{x}_j = (x_{j+1} - x_j) + \alpha(x_{j+1} - x_j)^2 - (x_j - x_{j-1}) - \alpha(x_j - x_{j-1})^2. \tag{2}$$

If we define $\mathbf{Q}$ and $\mathbf{P}$ such that

$$\mathbf{x} = A\mathbf{Q}, \quad \mathbf{p} = A\mathbf{P}, \tag{3}$$

where $\mathbf{x} = [x_1\ x_2\ \dots\ x_N]^T$, $\mathbf{p} = [p_1\ p_2\ \dots\ p_N]^T$, $\mathbf{Q} = [Q_1\ Q_2\ \dots\ Q_N]^T$, $\mathbf{P} = [P_1\ P_2\ \dots\ P_N]^T$, and

$$A = \sqrt{\frac{2}{N+1}} \begin{bmatrix} \sin\left(\frac{\pi}{N+1}\right) & \sin\left(\frac{2\pi}{N+1}\right) & \dots & \sin\left(\frac{N\pi}{N+1}\right) \\ \sin\left(\frac{2\pi}{N+1}\right) & \sin\left(\frac{4\pi}{N+1}\right) & \dots & \sin\left(\frac{2N\pi}{N+1}\right) \\ \vdots & \vdots & \ddots & \vdots \\ \sin\left(\frac{N\pi}{N+1}\right) & \sin\left(\frac{2N\pi}{N+1}\right) & \dots & \sin\left(\frac{N^2\pi}{N+1}\right) \end{bmatrix}, \tag{4}$$

we can rewrite Hamiltonian (1) in the form

$$H = \frac{1}{2}\sum_{k=1}^{N}\left(P_k^2 + \omega_k^2 Q_k^2\right) + \alpha H_3(Q_1, Q_2, \dots, Q_N), \tag{5}$$

where H_3 is a nonlinear function. Here, $\mathbf{Q}$ and $\mathbf{P}$ are the coordinates of the solution $\mathbf{x}$. Furthermore, the frequencies of the normal modes are given by the eigenvalues of A

$$\omega_k = 2\sin\left(\frac{k\pi}{2(N+1)}\right). \tag{6}$$

It is worth noting that the equations of motion in normal-mode coordinates are given by

$$\ddot{\mathbf{Q}} = D\mathbf{Q} + \alpha A^{-1}\mathbf{F}(\mathbf{Q}), \tag{7}$$

where

$$D = \begin{bmatrix} -\omega_1^2 & 0 & \dots & 0 \\ 0 & -\omega_2^2 & & 0 \\ \vdots & & \ddots & \vdots \\ 0 & 0 & \dots & -\omega_N^2 \end{bmatrix}, \quad \mathbf{F}(\mathbf{Q}) = \begin{bmatrix} f_1(\mathbf{Q}) \\ f_2(\mathbf{Q}) \\ \vdots \\ f_N(\mathbf{Q}) \end{bmatrix}.$$

In this context, $\mathbf{Q}$ is the spatial oscillation of the normal mode, while $\mathbf{P}$ is its velocity. Then, the energy of the k-mode can be defined by

$$E_k = \frac{1}{2}\left(P_k^2 + \omega_k^2 Q_k^2\right). \tag{8}$$

Using Eq. (8) in Eq. (5) yields

$$H = \sum_{k=1}^{N} E_k + \alpha H_3(Q_1, Q_2, \dots, Q_N).$$

For a relatively small nonlinear strength α, we have

$$H \approx \sum_{k=1}^{N} E_k.$$

From Eq. (7), we can see that the normal-mode transformation diagonalizes (uncouples) the equations of motion of the linear Hamiltonian system, i.e., the Hamiltonian system (1) with $\alpha = 0$. However, the nonlinear system with $\alpha > 0$ allows for energy sharing among various normal modes. In their original work, Fermi, Pasta, Ulam, and Tsingou [1] excited the mode with $k = 1$ by considering the following initial conditions

$$x_j = \sin\left(\frac{\pi j}{N+1}\right), \quad p_j = 0, \; j = 1, 2, \ldots, N. \tag{9}$$

In terms of normal-mode coordinates, this problem corresponds to solving Eq. (7) with initial conditions $Q_1 = \sqrt{(N+1)/2}$, $Q_k = 0$ for $k = 2, 3, \ldots, N$, and $\dot{Q}_k = 0$ for $k = 1, 2, \ldots, N$. Fermi, Pasta, Ulam, and Tsingou expected the energy to flow continuously and gradually from the initially excited mode up to the higher-order (higher k) normal modes. This process would continue until the system would reach energy equipartition. Surprisingly, they found that the energy was only shared among the first few modes before the system returned very close to its original configuration. This phenomenon is called the FPUT recurrence, and the discrepancy between expectations and numerical results is regarded as the FPUT paradox. An example of this phenomenon is shown in Fig. 1 for $N = 32$ with initial energy $E = 0.07471$. Particularly, Fig. 1(a) shows the solution of Eq. (2) under the initial conditions (9), which corresponds to the initial energy $E = 0.07471$. The resulting normal-mode energy for the first four modes (i.e., for $k = 1, \ldots, 4$) is shown in Fig. 1(b), where the repeating peak of the first mode occurs at approximately $t = 10^4$.

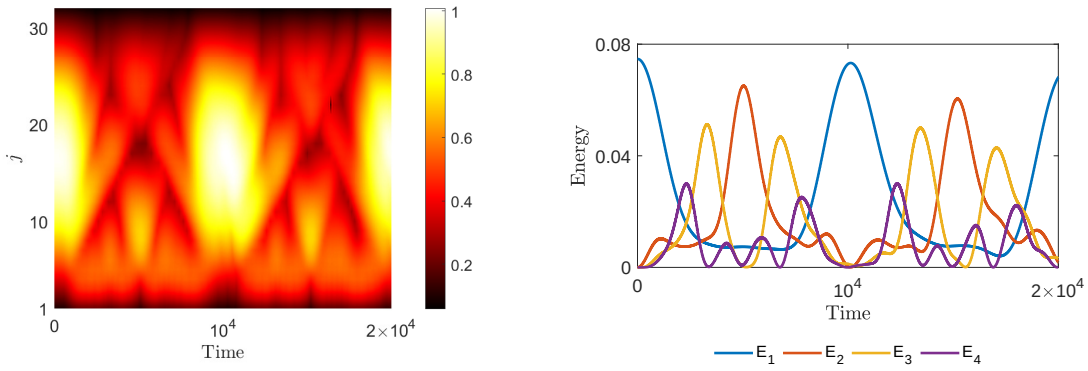

(a) (b)

Figure 1: The evolution of $x_j(t)$ of the Hamiltonian system (1) with $N = 32$ and initial energy $E = 0.07471$ using the initial condition in (9), where the top view of the oscillation envelop has been plotted in panel (a), and its corresponding energy (8) for the first four normal modes ($k = 1, \ldots, 4$) in panel (b). The FPUT recurrences can be seen in panel (b), where the energy returns to the initially excited mode at approximately $t = 10^4$ (second maximum of E_1). Note that the numbers on the vertical axis in panel (a) are the number of particles from 1 to $N = 32$.

Shortly, at a fixed number of particles, the picture is the following. The time of equipartition, as a function of initial energy, is plotted in Figure 8 of [14]. Then, it is proved as a consequence of the Kolmogorov-Arnold-Moser theorem that for energy small enough, a large measure of initial data evolves with quasi-periodic motion for all times. The applicability of such a result is due to Rink for the β model [15] and then by Henrici and Kappeler for an odd number of particles [16] and for an even number of particles too [17]. Then, the "metastable scenario" consists of the quasi-recurrence

phenomenon for a certain (eventually large) time scale. This is rigorously proved to occur for energy low enough either referring to the Korteweg-de Vries equation as an integrable model (see, e.g., [18] and, more recently, [19, 20, 21, 22]) or in relation with the Toda chain (see, e.g., [23, 24, 25, 26] and references therein). For these higher values of initial energy, one numerically sees equipartition to occur after a sufficiently long time, and, therefore, the recurrence phenomenon disappears.

3. Variability in the FPUT-α Hamiltonian

Let us consider now the FPUT-α system with variability whose Hamiltonian function is

$$H(x,p) = \sum_{j=0}^{N} \frac{1}{2}\frac{p_j^2}{t_j} + \sum_{j=0}^{N} \frac{1}{2}\left(t_{j+1}x_{j+1} - t_j x_j\right)^2 + \frac{\alpha}{3}\left(t_{j+1}x_{j+1} - t_j x_j\right)^3 = E, \tag{10}$$

with fixed boundary conditions $x_0 = x_{N+1} = 0$. Here, the variabilities t_j are picked at random in the following way: for a tolerance $\tau\%$, the values of t_j are drawn from a Gaussian distribution with mean 1 and standard deviation $\sigma = 1/3 \times 0.01\tau$. As a result, 99.73% the values of t_j would fall within the range $[1 - 0.01\tau, 1 + 0.01\tau]$ [4]. Then, the equations of motion follow as

$$\ddot{x}_j = t_{j-1}x_{j-1} - 2t_j x_j + t_{j+1}x_{j+1} + \alpha\left((t_{j+1}x_{j+1} - t_j x_j)^2 - (t_j x_j - t_{j-1}x_{j-1})^2\right). \tag{11}$$

Note that introducing $\tilde{x}_j = t_j x_j$, Eq. (11) becomes

$$\frac{1}{t_j}\ddot{\tilde{x}}_j = \tilde{x}_{j-1} - 2\tilde{x}_j + \tilde{x}_{j+1} + \alpha\left((\tilde{x}_{j+1} - \tilde{x}_j)^2 - (\tilde{x}_j - \tilde{x}_{j-1})^2\right), \tag{12}$$

with Hamiltonian

$$\hat{H}(\tilde{x},\tilde{p}) = \sum_{j=0}^{N} \frac{t_j}{2}\tilde{p}_j^2 + \sum_{j=0}^{N}\left[\frac{1}{2}(\tilde{x}_{j+1} - \tilde{x}_j)^2 + \frac{\alpha}{3}(\tilde{x}_{j+1} - \tilde{x}_j)^3\right], \tag{13}$$

where $\tilde{p}_j = p_j/t_j$ in Eq. (10). Equation (12) is nothing but the disordered FPUT lattice with mass $m_j = 1/t_j$ (see, e.g., [27] for an early study on normal mode frequencies of harmonic lattices with random masses). In this report, we will work with Eq. (11) because it is convenient numerically, especially when some $|t_j|$ becomes small (i.e., m_j becomes large).

Equation (11) can be written in the matrix form

$$\ddot{\mathbf{x}} = S\mathbf{x} + \alpha\mathbf{F}(\mathbf{x}), \tag{14}$$

where

$$\ddot{\mathbf{x}} = \begin{bmatrix} \ddot{x}_1 \\ \ddot{x}_2 \\ \ddot{x}_3 \\ \vdots \\ \ddot{x}_N \end{bmatrix}, \ \mathbf{x} = \begin{bmatrix} x_1 \\ x_2 \\ x_3 \\ \vdots \\ x_N \end{bmatrix}, \ S = \begin{bmatrix} -2t_1 & t_2 & 0 & & \dots & 0 \\ t_1 & -2t_2 & t_3 & & & 0 \\ \vdots & & & \ddots & & \vdots \\ 0 & & \dots & t_{N-2} & -2t_{N-1} & t_N \\ 0 & & & 0 & t_{N-1} & -2t_N \end{bmatrix},$$

and $\mathbf{F}$ is some nonlinear vector function. Let

$$V = [v_1 \ \ v_2 \ \ \cdots \ \ v_N] \tag{15}$$

denote a matrix where its columns v_i are the eigenvectors of S with $\|v_i\| = 1,\ i = 1, \ldots, N$ and the corresponding eigenvalues $\lambda_1, \lambda_2, \ldots, \lambda_N$. For convenience, let

$$\lambda_k = -\hat{\omega}_k^2,\ k = 1, \ldots, N, \tag{16}$$

where $\hat{\omega}_k \in \mathbb{R}$.

Note that $t_j = 1$ for all j in the FPUT-α system without variability, so S becomes a tridiagonal matrix. In this case, V is similar to A and $\lambda_k = -\omega_k^2,\ k = 1, \ldots, N$, given in Eq. (6)[28].

Introducing the normal-mode transformation

$$\mathbf{x} = M\mathbf{Q}, \tag{17a}$$

$$\mathbf{p}' = M\mathbf{P}, \tag{17b}$$

where $p'_j = p_j/t_j$, $M = kV$, and $k = c\hat{\omega}_1/\sqrt{2E}$ for some constant $c \in \mathbb{R}$, the equations of motion (14) become

$$\ddot{\mathbf{Q}} = D\mathbf{Q} + \alpha M^{-1}\hat{\mathbf{F}}(\mathbf{Q}), \tag{18}$$

where D is a diagonal matrix with diagonal entries given by the eigenvalues of S and $\hat{\mathbf{F}}$ a nonlinear vector function. Similarly to the previous section, the energy of normal-mode k is given by

$$E_k = \frac{1}{2}\left(P_k^2 + \hat{\omega}_k^2 Q_k^2\right). \tag{19}$$

Next, we investigate the influence of variability on the evolution of the normal-mode energy at a fixed energy level, following [1]. In the same spirit as the original FPUT experiment, we choose the initial conditions in the physical space such that only the lowest mode is excited. The initial energy employed in our computations is equal to the initial energy of the original FPUT-α system in Eq. (1) under the initial conditions (9) for each number of particles N. Then, the initial conditions in Eq. (11) are chosen by finding a constant $c \in \mathbb{R}$ such that

$$\mathbf{x}(0) = cv_1, \quad \mathbf{p}(0) = 0, \tag{20}$$

satisfy Eq. (10) for a fixed energy E, which was obtained previously. In this context, v_1 refers to the first column of matrix V as defined in Eq. (15). We note that in the normal-mode space, the initial conditions read as

$$Q_1(0) = \frac{\sqrt{2E}}{\hat{\omega}_1}, \quad Q_k(0) = 0,\ k = 2, \ldots, N, \quad P_j(0) = 0,\ j = 1, \ldots, N. \tag{21}$$

The time evolution of the solutions to system (11) with initial conditions (20) and its associated normal-mode energy E_k of the first four modes for $N = 32$ particles and three different percentages of tolerance, namely $\tau = 5\%$, $\tau = 50\%$ and $\tau = 95\%$, are shown in Fig. 2. The initial energy of the system is $E = 0.07471$, which is similar to the initial energy in Fig. 1. Comparing panel (b) in Figs. 1 and panels (b), (d), (f) in Fig. 2, we can see that the recurrence is weakening due to the effect of variability, as evidenced by the declining peak of the mode energy E_1. Then, as the variability increases, it becomes more difficult to transmit energy from the lowest to the higher modes, resulting in the localization of energy, shown in panels (d) and (f) in Fig. 2.

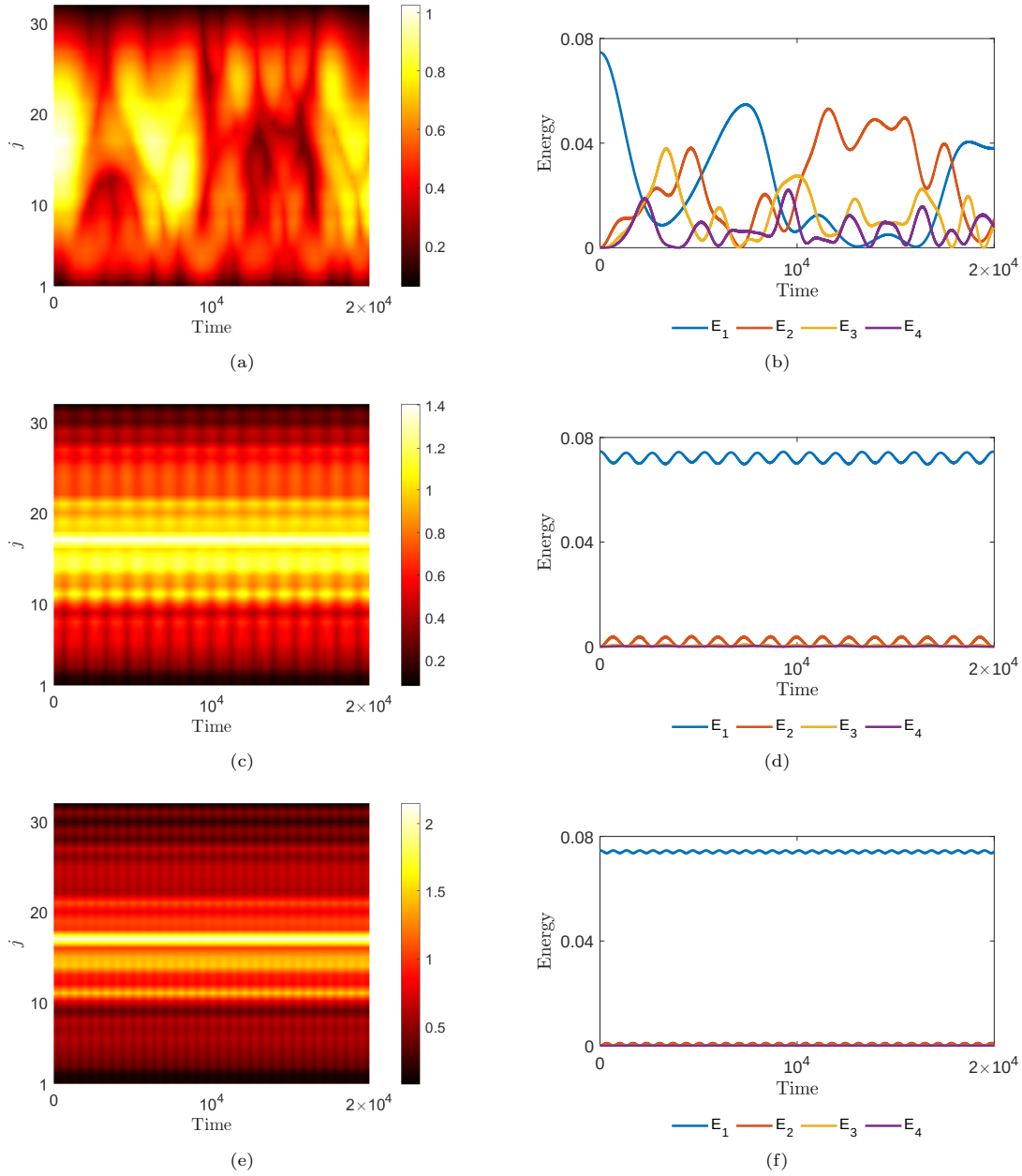

Figure 2: Evolution of the energy E for the first four normal modes for the system in Eq. (11) with $N = 32$ particles. Panels (a) and (b) are for $\tau = 5\%$ tolerance, panels (c) and (d) for $\tau = 50\%$ and panels (e) and (f) for $\tau = 95\%$ tolerance. Note that the numbers on the vertical axes in panels (a), (c), (e) are the number of particles from 1 to $N = 32$.

In the next section, we will explain why the energy exchange across normal modes decreases as the percentage of variability increases. As a result, energy localization takes place in the energy-mode space. The plots of normal-mode energies show that in the event of energy localization, most of the normal-mode coordinates vanish in time. Thus, rather than working in real (physical) space, it would be advantageous to work in the normal-mode coordinate system, given in Eq. (18), as we can approximate system (18) by taking into account only the first few normal modes. We present in Fig. 3 the normal-mode energy from the approximation of Eq. (18) using 2, 4, and 8 normal modes, while all other modes are fixed at 0, and using different percentages of variability to demonstrate numerically that this approximation can be justified.

In terms of energy-recurrence period, we can observe in Fig. 3 that using 4 and 8 normal modes produces dynamics that are nearly identical to those seen in Figs. 1 in the absence of variability. We can detect energy recurrence and localization even with 2 normal modes as the percentage of variability increases. We can see in panels (d) and (f) in Fig. 2 and panels (g) and (j) in Fig. 3 that a two normal-mode system yields an adequate approximation to Eq. (18). Therefore, we will look at these two normal-mode approximations in the following section.

4. Two normal-mode approximation

The majority of high-order modes are negligible when energy localization takes place, as illustrated in Fig. 2. Therefore, we set all high-order normal-mode values to zero, except the first two, to obtain a two normal-mode approximation. In practice, we set $Q_k(t) = 0$ for $k = 3, 4, \ldots, N$ in Eq. (18). This gives us the following system

$$\ddot{Q}_1 = -\hat{\omega}_1^2 Q_1 + \epsilon \left(A_1 Q_1^2 + A_2 Q_2^2 + A_3 Q_1 Q_2 \right), \tag{22a}$$

$$\ddot{Q}_2 = -\hat{\omega}_2^2 Q_2 + \epsilon \left(B_1 Q_1^2 + B_2 Q_2^2 + B_3 Q_1 Q_2 \right), \tag{22b}$$

where $A_i,\ B_i \in \mathbb{R},\ i = 1, 2, 3$ and $\hat{\omega}_k$ is given in Eq. (16).

4.1. Multiple-scale expansions

We consider the following asymptotic series

$$Q_1 = X_0(t, T) + \epsilon X_1(t, T) + \ldots, \tag{23a}$$

$$Q_2 = Y_0(t, T) + \epsilon Y_1(t, T) + \ldots, \tag{23b}$$

where $\hat{\omega}_2 = 2\hat{\omega}_1 + \epsilon$, $|\epsilon| \ll 1$, and $T = \epsilon t$ is a slow-time variable. The leading-order approximations to Eqs. (23) are given by

$$X_0 = q_1(T) e^{i\hat{\omega}_1 t} + q_1^*(T) e^{-i\hat{\omega}_1 t}, \quad Y_0 = q_2(T) e^{i\hat{\omega}_2 t} + q_2^*(T) e^{-i\hat{\omega}_2 t}, \tag{24}$$

where i is the imaginary unit of the complex numbers, i.e., $i^2 = -1$. Substituting Eqs. (23), (24) into Eq. (22), expanding the equations in ϵ, and applying the standard solvability condition to avoid secular terms appearing (see, e.g., [29]), we obtain

$$i \frac{dq_1(T)}{dT} = q_1(T) + \widetilde{A} q_1^* q_2, \tag{25a}$$

$$i \frac{dq_2(T)}{dT} = q_2(T) + \widetilde{B} q_1^2, \tag{25b}$$

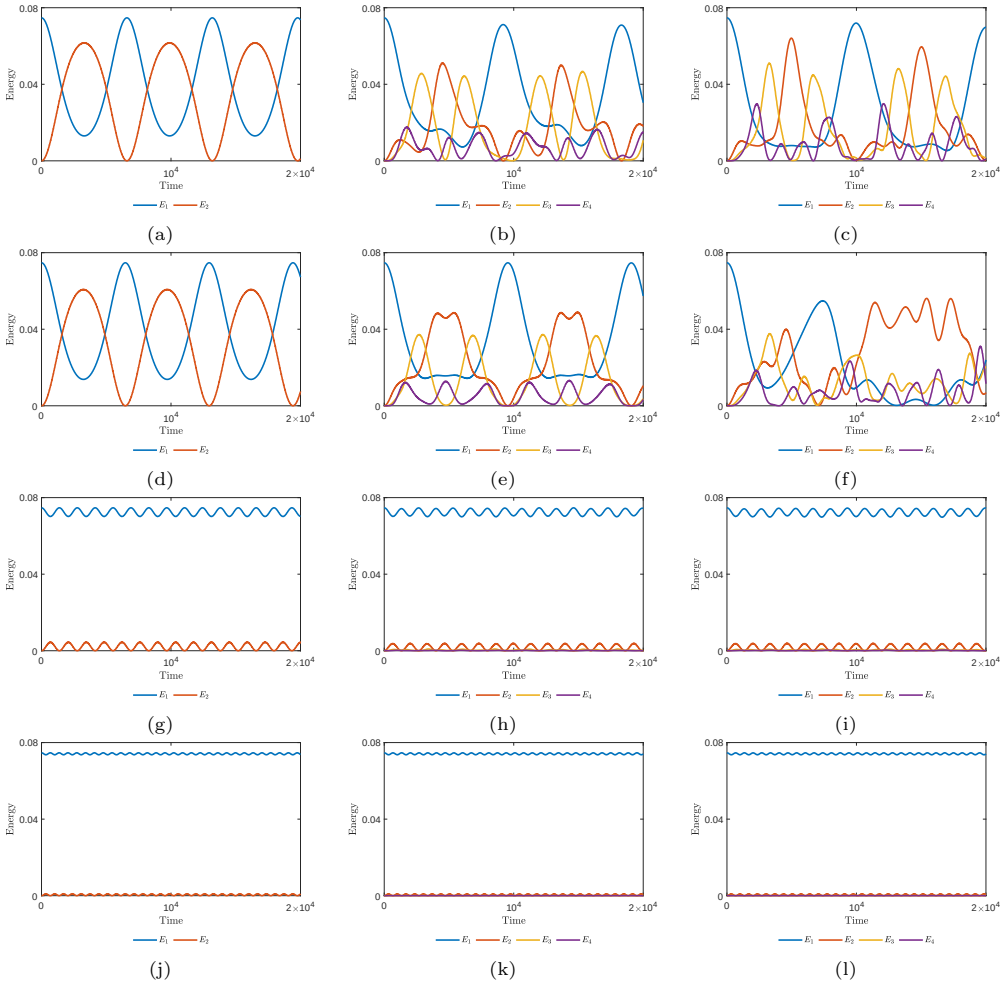

Figure 3: The evolution of normal-mode energy as obtained from integrating Eq. (18) using different normal-mode numbers. In panels (a), (d), (g), and (j), two normal modes are used; in panels (b), (e), (h), and (k), four modes are used, and in panels (c), (f), (i), and (l), eight modes are used. Each row represents different amounts of tolerance, i.e. 0% (panels (a)-(c)), 5% (panels (d)-(f)), 50% (panels (g)-(i)), and 95% (panels (j)-(l)). The first four modes, except for the two normal-mode system, are plotted in all panels, but they are active for 0% and 5% tolerance in panels (a) and (f). For 95% tolerance, all modes except the first, are essentially 0.

for q_1 and q_2, respectively, where $\tilde{A} = A_3/(2\hat{\omega}_1)$ and $\tilde{B} = B_1/(2\hat{\omega}_2)$. Recalling Eqs. (21), the initial conditions of system (25) are

$$q_1(0) = \frac{Q_1(0)}{2}, \quad q_2(0) = 0. \tag{26}$$

Our numerical computations show that both $\tilde{A}$ and $\tilde{B}$ in Eq. (25), which are functions of τ, are either positive or negative for fixed τ. However, Eq. (25) is invariant when $\tilde{A}$ and $\tilde{B}$ have the same sign, as we can use the transformation $\hat{q}_2 = -q_2$. Therefore, we plot these parameters when both $\tilde{A}$ and $\tilde{B}$ are positive only as a function of τ for $N = 32$ particles and 100 realizations in Fig. 4. These realizations have been computed by fixing τ and then opting for 100 sets of $N = 32$ randomly generated numbers.

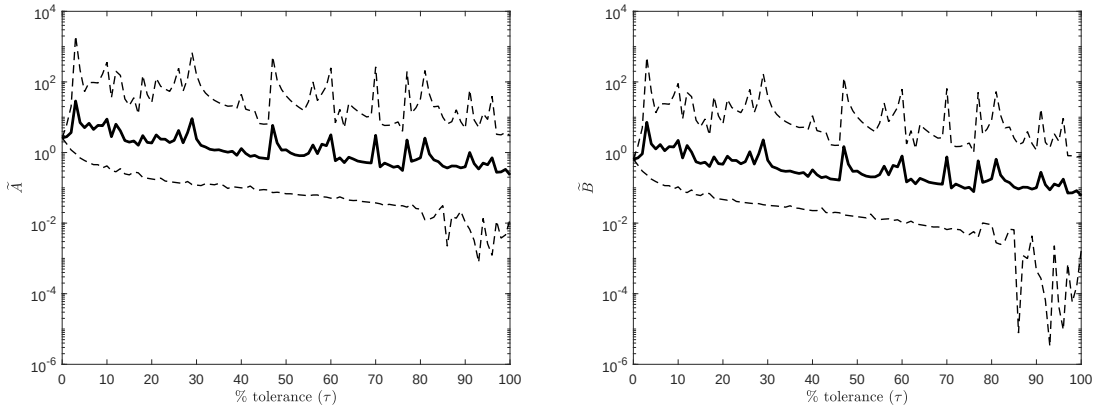

(a) (b)

Figure 4: The parameter values $\tilde{A}$ and $\tilde{B}$ as a function of τ obtained numerically for $N = 32$. The solid black curve is the parameter mean over 100 sets of variabilities at the same percentage, and the upper and lower black dashed curve are their maximum and minimum values, respectively. Note the logarithmic scale on the vertical axis and that both $\tilde{A}$ and $\tilde{B}$ are always positive (see discussion in the text).

We compare the dynamics of normal modes Q_1 and Q_2 of Eq. (22) and its slow-time variable approximations q_1 and q_2 of Eqs. (25) in Fig. 5, where it can be seen that q_j is an envelope of Q_j for $j = 1, 2$.

Next, we describe the mechanism of energy localization when the percentage of variability τ increases. It is worth noting that as $q_2(0) = 0$, the energy transmission from $q_1(t)$ to $q_2(t)$ is made possible due to the nonlinear coupling coefficient $\tilde{B}$. Therefore, we will analyze the role of $\tilde{B}$ in energy localization as we increase τ.

4.2. Equilibrium solutions

To analyze the equilibrium solutions of the envelope equations (25), it is practical to write q_1 and q_2 in polar form $q_1 = r_1 e^{i\phi_1}$ and $q_2 = r_2 e^{2i\phi_2}$, where $r_1 = |q_1|$, $r_2 = |q_2|$. We then define the new variables

$$P = r_1^2 + r_2^2, \tag{27a}$$

$$\Delta = r_1^2 - r_2^2, \tag{27b}$$

$$\theta = \phi_2 - \phi_1. \tag{27c}$$

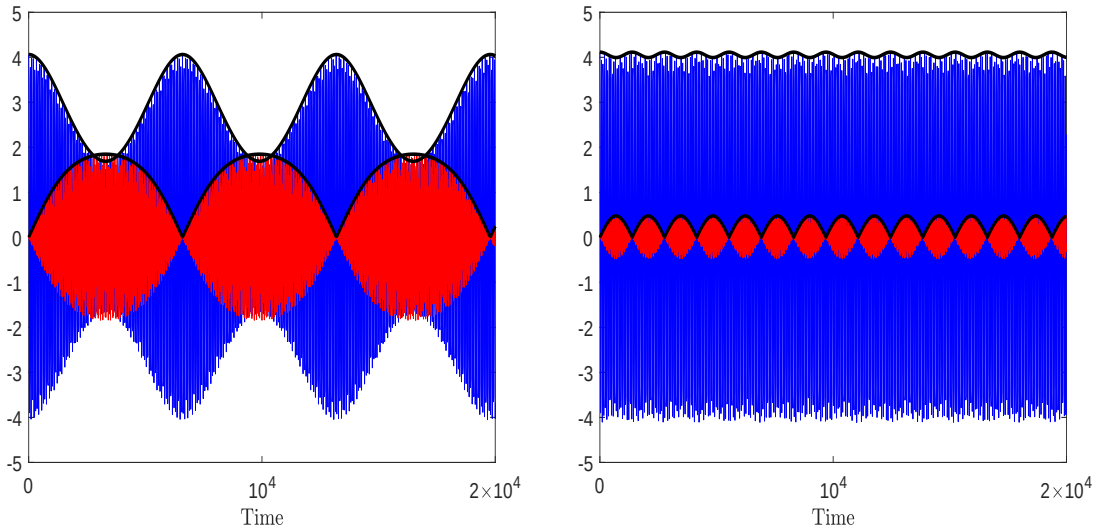

Figure 5: Plot of the evolution of normal-mode variables Q_1 (blue curve) and Q_2 (red curve) in time with their envelopes q_1 and q_2 (black curves) from Eqs. (25) for $\tau = 0\%$ in panel (a) and $\tau = 50\%$ in panel (b).

Substituting Eqs. (27) into Eqs. (25), we derive the following set of equations (a similar derivation can be found in [30])

$$\dot{P} = \frac{\widetilde{A} - \widetilde{B}}{\widetilde{A} + \widetilde{B}} \dot{\Delta}, \tag{28a}$$

$$\dot{\Delta} = \frac{\sqrt{2\,(P-\Delta)}\sin(2\,\theta)\,(P+\Delta)\left(\widetilde{A}+\widetilde{B}\right)}{2}, \tag{28b}$$

$$\dot{\theta} = -\frac{2\,\widetilde{A}\cos(2\,\theta)\,(\Delta - P) + \widetilde{B}\cos(2\,\theta)\,(\Delta + P) - \sqrt{2\,(P-\Delta)}}{2\sqrt{2\,(P-\Delta)}}. \tag{28c}$$

Integrating Eq. (28a), we obtain the constant of motion C, where

$$C = P - \frac{\widetilde{A} - \widetilde{B}}{\widetilde{A} + \widetilde{B}} \Delta.$$

First, we will study the stability of the equilibria of the reduced system in Eqs. (28b), (28c). Then, we will discuss the stability of the equilibria of its corresponding system given in Eq. (25). To study the reduced system of Eqs. (28b), (28c), we restrict the phase difference θ in the interval $0 \leq \theta < \pi$ and obtain two equilibria, namely (θ_j, Δ_j), $j = 1, 2$. The θ_j equilibria depend on $\tilde{A}$ and $\tilde{B}$, and are given by

1. if $\tilde{A} > 0$ and $\tilde{B} > 0$ or $\tilde{A} < 0$ and $\tilde{B} < 0$ then $\theta_1 = 0$ and $\theta_2 = \pi/2$
2. if $\tilde{A} > 0$ and $\tilde{B} < 0$, then $\theta_1 = \theta_2 = \pi/2$
3. if $\tilde{A} < 0$ and $\tilde{B} > 0$, then $\theta_1 = \theta_2 = 0$.

Furthermore, Δ_j equilibria, for $j = 1, 2$, are

$$\Delta_j = \frac{\left(6\,\widetilde{A}^2C - 3\,\widetilde{A}\widetilde{B}C - (-1)^j\sqrt{1 + 6\,\widetilde{A}\left(\widetilde{A} + \widetilde{B}\right)C} - 1\right)\left(\widetilde{A} + \widetilde{B}\right)}{18\widetilde{A}^2\widetilde{B}}. \tag{29}$$

Next, we study the stability of the equilibria, which is determined by the eigenvalues of the Jacobian matrix of Eqs. (28b), (28c), evaluated at the equilibria, i.e., by

$$\lambda_{1,2}^{(j)} = \pm\frac{\sqrt{-3 - 18\widetilde{A}^2C - 18\widetilde{A}\widetilde{B}C + 6(-1)^j\sqrt{1 + 6\,\widetilde{A}\left(\widetilde{A} + \widetilde{B}\right)C}}}{3}. \tag{30}$$

Equation (29) implies that the equilibria exist when

$$1 + 6\,\widetilde{A}\left(\widetilde{A} + \widetilde{B}\right)C \geq 0. \tag{31}$$

Using the initial conditions in Eq. (26), Eq. (31) becomes

$$1 + 12\widetilde{A}\widetilde{B}r_1^2 \geq 0.$$

Therefore, the threshold for the existence of the equilibrium is given by

$$1 + 12\widetilde{A}\widetilde{B}r_1^2 = 0,$$

depicted by the blue curve in Fig. 6. The solid and dashed lines represent the curve below and above the line $\widetilde{A} + \widetilde{B} = 0$, respectively. The black dashed line represents the line $\widetilde{A} + \widetilde{B} = 0$.

When an equilibrium exists, the eigenvalues given in Eq. (30) are either real or purely imaginary, indicating that the equilibria are a saddle-node or a centre. Using the initial conditions in Eqs. (26), the thresholds that separate between real and purely imaginary eigenvalues are

$$1 + 12\widetilde{A}\widetilde{B}r_1^2 = 0, \tag{32}$$

$$1 - 4\widetilde{A}\widetilde{B}r_1^2 = 0. \tag{33}$$

We plot in Fig. 6, Eqs. (32) and (33) as blue and red curves, respectively.

System (28) with parameter values $\widetilde{A}$ and $\widetilde{B}$ above the red curve in the first quadrant or below the red curve in the third quadrant in Fig. 6 has two equilibria given in Eq. (29), which are both centres and therefore stable. Conversely, if both parameters lie between the two red curves, then one equilibrium is a centre, and the other a saddle-node.

Next, we will discuss the stability of the equilibria of Eq. (25). As this system can be transformed into Eqs. (28b) and (28c) in terms of Δ and θ, we utilize Eqs. (28b) and (28c) to describe the dynamics of Eq. (25). Equations (28) are obtained from Eqs. (25) by using Eqs. (27), where both r_1 and r_2 are non-negative real numbers. Equation (28) requires $P - \Delta > 0$ to have real solutions, whereas Eq. (27) requires $P - \Delta \geq 0$ and $P + \Delta \geq 0$, otherwise r_1 and r_2 will be complex numbers. The region that fulfils these two inequalities is referred to as the well-defined region and is represented by the shaded area in Fig. 6. For instance, the well-defined region in the first quadrant is bounded. There are two equilibria in the region above the red curve, while there is only one in

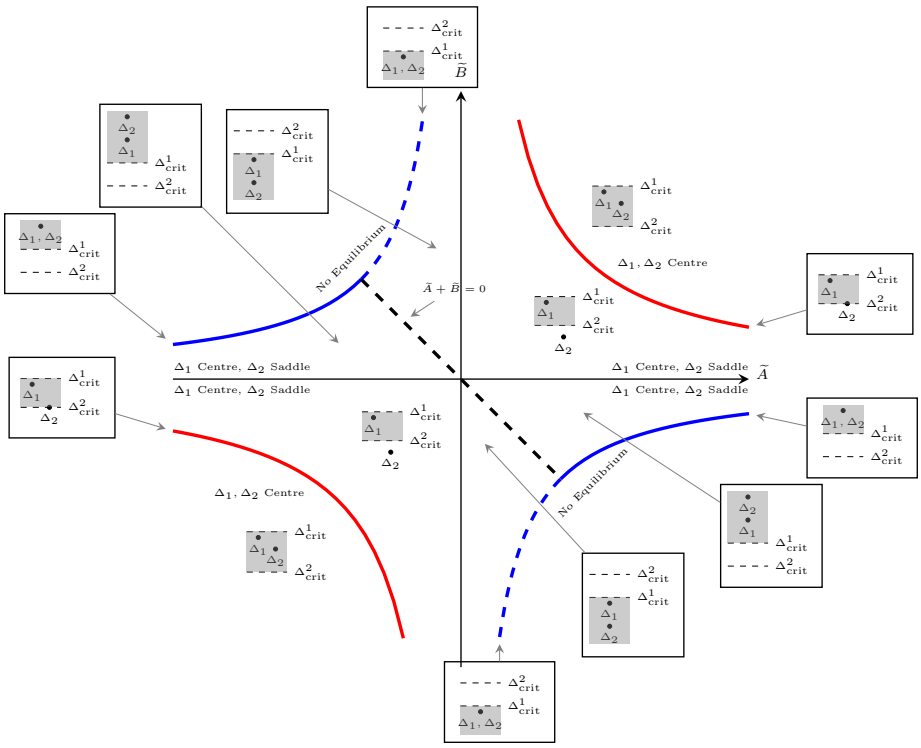

Figure 6: Bifurcation diagram of the equilibria Δ_1 and Δ_2 in the $(\widetilde{A}, \widetilde{B})$-space. The well-defined region for system (25) is shown as the shaded area (see text for more details).

the region below it. This means that Eqs. (25) and (28) have two equilibria in the region above the red curve, whereas they share only one equilibrium in the region below it as Δ_2 lies outside the shaded region. To determine the boundary for Δ in the well-defined region, we solve the inequalities $P-\Delta>0$ and $P+\Delta\geq 0$, which depend on $\widetilde{A}$ and $\widetilde{B}$, as follow

- If $\frac{\widetilde{A}-\widetilde{B}}{\widetilde{A}+\widetilde{B}}\geq 1$, then $\Delta>\max\left\{\Delta^1_{\text{crit}},\Delta^2_{\text{crit}}\right\}$, where

$$\Delta^1_{\text{crit}}=\frac{C\left(\widetilde{A}+\widetilde{B}\right)}{2\widetilde{B}} \text{ and } \Delta^2_{\text{crit}}=-\frac{C\left(\widetilde{A}+\widetilde{B}\right)}{2\widetilde{A}}.$$

- If $-1\leq\frac{\widetilde{A}-\widetilde{B}}{\widetilde{A}+\widetilde{B}}<1$, then $\Delta^2_{\text{crit}}\leq\Delta<\Delta^1_{\text{crit}}$.

- If $\frac{\widetilde{A}-\widetilde{B}}{\widetilde{A}+\widetilde{B}}<-1$, then $\Delta<\min\left\{\Delta^1_{\text{crit}},\Delta^2_{\text{crit}}\right\}$.

All types of the well-defined region in the ($\tilde{A}$,$\tilde{B}$)-plane are depicted in Fig. 6. We also plot the equilibria $\Delta_j, j=1,2$ and their nature in Fig. 6. Moreover, the values of Δ_j are plotted in Fig. 7. We plot in Fig. 7 (b) $\tanh(\Delta_2/100)$ rather than Δ_2 to better illustrate Δ_2 as it approaches infinity when $\widetilde{A}$ or $\widetilde{B}$ approach zero.

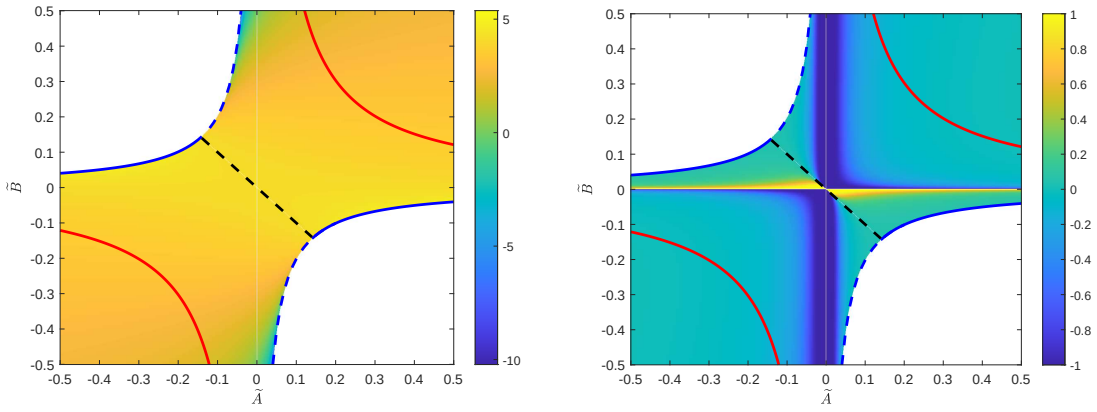

(a) (b)

Figure 7: The color plot of Δ_1 (in panel (a)) and $\tanh(\Delta_2/100)$ (in panel (b)) as a function of $\widetilde{A}$ and $\widetilde{B}$. Note that the red, black dashed, and blue curves are the same curves as those in Fig. 6.

According to Fig. 4, we have obtained numerically that the parameter values for Eq. (25) are either both positive or negative. Therefore, this equation can only occupy the first and third quadrants in Fig. 6. If both parameter values are positive (negative), then for a small percentage of variability, both will be located above (below) the red curve in Fig. 6. In this case, Eq. (25) will have two equilibria where both of them are centers, hence stable. Upon increasing the percentage of variability further, both parameter values decrease, and at some percentage, they cross the red curve. In this case, Eq. (25) will only have one stable equilibrium: a center. These two cases' phase space is shown in Fig. 8. For $\tau=0\%$ or in the absence of variability, the parameter values are $\widetilde{A}=2.58$ and $\widetilde{B}=0.65$. The two stable equilibria are $(\theta_1,\Delta_1)=(0,2.74)$ and $(\theta_2,\Delta_2)=(\pi/2,1.98)$,

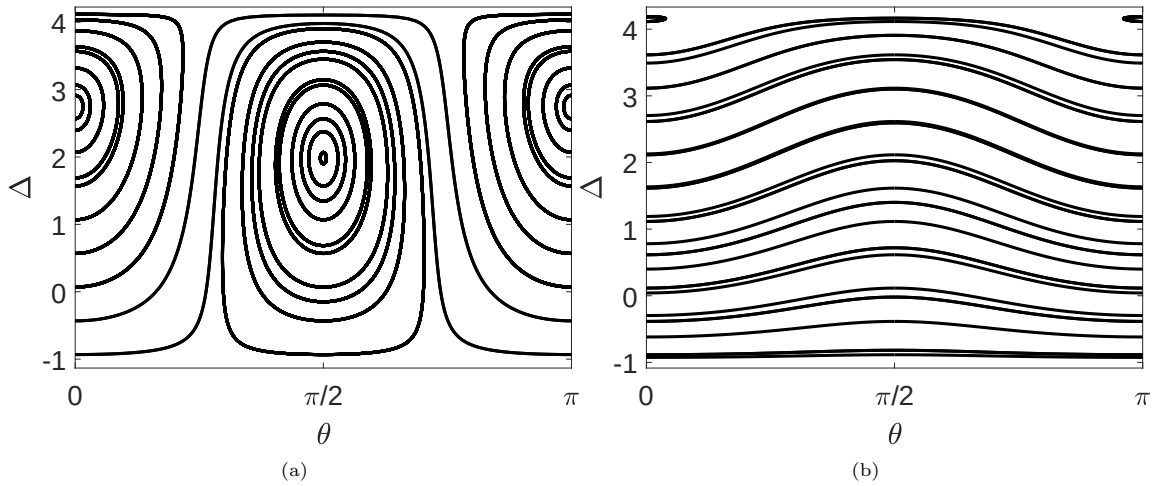

(a) (b)

Figure 8: Phase portraits of the (Δ, θ) system given by Eqs. (28b), (28c) for $\tau = 0\%$ in panel (a) and $\tau = 50\%$ in panel (b).

which are shown in Fig. 8a. For $\tau = 50\%$, the parameter values are $\widetilde{A} = 0.13$ and $\widetilde{B} = 0.03$. The stable equilibrium is $(\theta_1, \Delta_1) = (0, 4.16)$, which is shown in Fig. 8b. We can also determine the boundary of the well-defined region as

$$\lim_{\widetilde{B}\to 0} \Delta^1_{\text{crit}} = r_1^2, \quad \lim_{\widetilde{B}\to 0} \Delta^2_{\text{crit}} = 0, \tag{34}$$

where we have used the initial conditions (26) in the limit computations. Equation (34) tells us that Δ in the well-defined region is positive definite as $\widetilde{B} \to 0$. Recalling Eq. (27b), we conclude that $\Delta > 0$ corresponds to energy localization as the magnitude of q_1 is always greater than q_2.

5. Effect of variability on dynamics

The FPUT-α system can be considered a truncation of the regular, integrable Toda system. As a result, the non-integrable FPUT-α system acts similarly to the integrable Toda system for a period of time before exhibiting non-integrable behavior [31]. The length of this period, also known as the lifetime of the metastable state, depends on the energy E and the number of particles N [32]. For a small initial energy, the FPUT-α system persists in the metastable state for a long time, causing energy thermalization to be difficult to observe numerically.

It was concluded in [32] that the lifetime of the metastable state t_m follows the scaling law $t_m = 0.023 \times (E\alpha^2)^{-4.9}$, while according to [33] (see, e.g., Fig. 1 therein) or [34] (see its Fig. 5), it was rather $t_m \sim (\alpha^2 E/N)^{-5/4}$. Using those results as a mere guide, we expect to observe the regular dynamics of the FPUT-α system (1) for $t \lesssim t_m$. Here, we keep the energy of system (10) fixed and study how variability affects its dynamics. Particularly, we look at lattices of $N = 4, 8, 16, 32$ particles in systems (1) (with no variability) and (10) (with variability) and utilize the maximum Lyapunov exponent (mLE) [35, 36] to distinguish between regular and chaotic dynamics.

To calculate the mLE, we follow the trajectory of an initial condition

$$\mathbf{x}(0) = (q_1(0), \ldots, q_N(0), p_1(0), \ldots, p_N(0)),$$

as it evolves according to Hamilton's equations of motion

$$\dot{\mathbf{x}} = \mathbf{f}(\mathbf{x}) = \left[\frac{\partial H}{\partial \mathbf{p}} \quad -\frac{\partial H}{\partial \mathbf{q}}\right]^T,$$

and an accompanying deviation vector

$$\mathbf{w}(0) = (\delta q_1(0), \ldots, \delta q_N(0), \delta p_1(0), \ldots, \delta p_N(0)),$$

that evolves according to the variational equation

$$\dot{\mathbf{w}} = \frac{\partial \mathbf{f}}{\partial \mathbf{x}}(\mathbf{x}(t)) \cdot \mathbf{w}. \tag{35}$$

Then, mLE is defined by

$$\lambda = \lim_{t\to\infty} \frac{1}{t} \ln \frac{||\mathbf{w}(t)||}{||\mathbf{w}(0)||},$$

where ln is the natural logarithm. If mLE approaches zero following the law $1/t$, its trajectory is regular; otherwise, if it converges to a positive value over time, then its trajectory is chaotic [36]. Therefore, plotting mLE in $\log_{10}$-$\log_{10}$ scale is especially useful since it provides a better visual aid, as the law $1/t$ is a line with a negative slope and serves as a guide to the eye. We use the tangent-map approach [37] and Yoshida's fourth-order symplectic integrator [38] to integrate the equations of motion (2) and (11) with their corresponding variational equations (following Eq. (35)). We found that a time step of 0.01 keeps the relative energy error to less than 10^{-8}. The final integration time in all of our calculations is $t = 10^8$.

First, we investigate the case where there is no variability, namely the FPUT-α system (1) with the equations of motion (2). We use the same initial condition in Eq. (9) for all N. This initial condition yields distinct energies for different N, i.e., $E = 0.4775$ for $N = 4$, $E = 0.2714$ for $N = 8$, $E = 0.1447$ for $N = 16$, and $E = 0.0747$ for $N = 32$. Our results in Fig. 9 indicate that all trajectories are regular up to $t = 10^8$, which is supported by the tendency of the mLEs to converge to zero following the $1/t$ law. These findings are consistent with the fact that energy recurrences in the homogeneous FPUT lattice (1) persist in the metastable state for exceptionally long periods of time, stalling the approach to energy equipartition [32]. This result provides direct, strong evidence that energy recurrences are generated by regular trajectories. This then means the system cannot reach energy equipartition.

Next, we consider the case with variability where the Hamiltonian is given in Eq. (10). For each number of particles N, the initial conditions are given in Eq. (20), where the initial energy is similar to that in the case without variability. We compute the mLE for 40 realizations of variability for $\tau = 5\%$, 50%, and 95%. For $N = 4$, all trajectories with $\tau = 5\%$, 50%, and 95% in panels (a)-(c) of 10 seem to be regular up to the final integration time $t = 10^8$, which is shown by the mLEs' tendency to converge to zero following the $1/t$ law. We see similar behavior for $N = 8$ and $\tau = 5\%$. However, when $\tau = 50\%$ and $\tau = 95\%$, there are three and four chaotic trajectories, respectively. The number of chaotic trajectories increases significantly for $N = 16$ and 32. The percentage of chaotic trajectories (out of 40 realizations) as a function of N is depicted in Fig. 11, where the increase is evident for $\tau = 5\%$ and 50%. Nevertheless, when $\tau = 95\%$, the proportion of chaotic trajectories only increases for $N = 4, 8, 16$ and then decreases when $N = 32$. These results imply

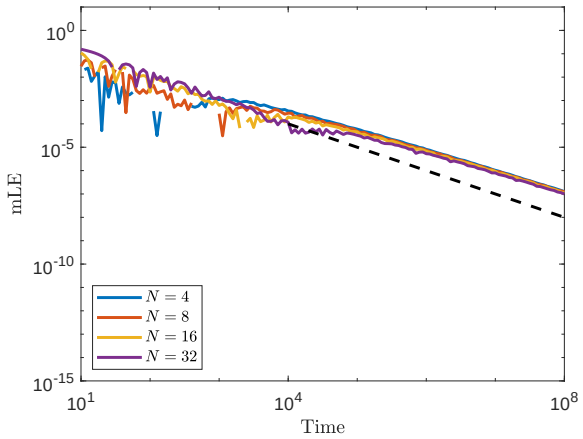

Figure 9: Plot of mLE over time for the range of N values shown in the insets (denoted by distinct colors) of the FPUT system (1). All axes are on a logarithmic scale. The dashed black line in panel (a) is the law of $1/t$ for regular trajectories to guide the eye.

that a small percentage of tolerance has less effect on chaotic behavior than a bigger percentage for small N, which is reversed when N increases.

Now, we want to study how energy localization relates to trajectories' chaotic characteristics. In the absence of variability, the appearance of super recurrence when we integrate Eq. (2) for a long time has been reported in [2, 39, 40, 3]. Therefore, the energy recurrence is an attribute of a regular trajectory according to Fig. 9. Regarding variability, system (10) contains chaotic and regular trajectories, which depend on N and τ. We find that either energy recurrence or energy localization occurs when the trajectory is regular. In contrast, chaotic trajectories correspond to the thermalization of energy. In Fig. 12, we illustrate a particular instance of mLE and its corresponding normal mode energy for $N = 16$ and $\tau = 5\%, 50\%, 95\%$, resulting from regular and chaotic trajectories. We use a similar initial energy as in Fig. 10, i.e. $E = 0.1447$.

The superrecurrence can be seen in panel (b) in Fig. 12 with a period of about 7×10^7, while panel (d) shows the localization of energy in the first few normal modes. This localization is getting stronger (no energy is transferred to other normal modes) if we consider the regular trajectory with a higher tolerance percentage τ. Furthermore, the thermalization of energy due to chaotic trajectories is shown in panel (f) in Fig. 12, where the energy is shared among all normal modes.

6. Conclusion

In this paper, we have considered the disordered FPUT-α system for fixed energies. Using a two-normal-mode approximation, which has been solved asymptotically by a multiple-scale expansion method, we have explained the mechanism for energy localization when the percentage of variability increases. While we only excited the first normal mode in this report, our preliminary results (not presented herein) also indicated that the conclusion still applies when a single higher mode is excited. Hence, simultaneously exciting two or more modes that are "far apart" would only result in "linear" dynamics (as the modes effectively do not interact with each other). The result that there is no energy sharing among normal modes when there is randomness in the FPUT lattice as in (11) with large enough variance σ, may therefore be formulated as the following conjecture:

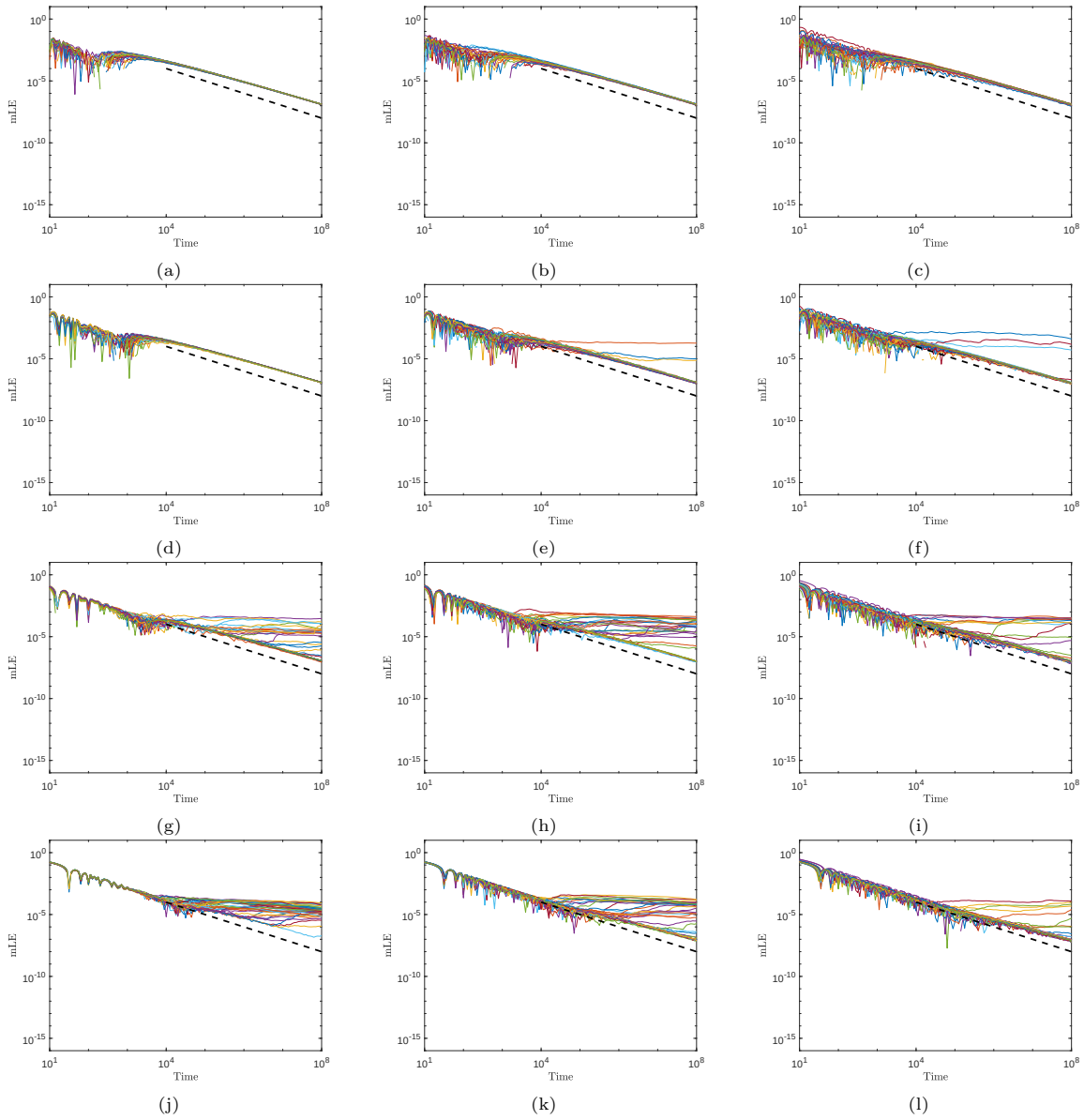

Figure 10: Plot of mLE for 40 trajectories (denoted by distinct colors) with $N = 4$ in panels (a)-(c), $N = 8$ in panels (d)-(f), $N = 16$ in panels (g)-(i), and $N = 32$ in panels (j)-(l). The tolerance is 5% in panels (a), (d), (g), (j), 50% in panels (b), (e), (h), (k), and 95% in panels (c), (f), (i), (l). All axes are on a logarithmic scale. The dashed black line in all panels is the law $1/t$ for regular trajectories to guide the eye.

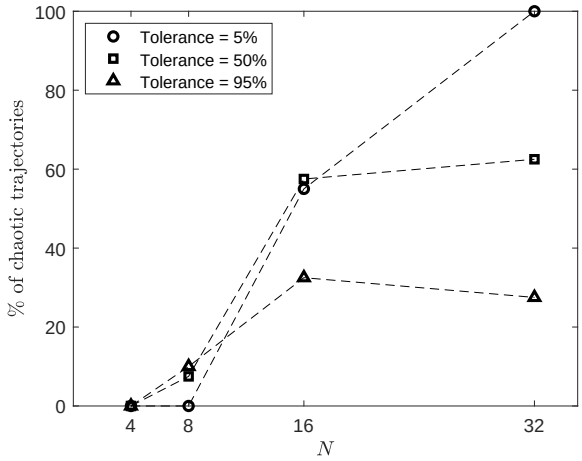

Figure 11: Percentage of chaotic trajectories as a function of N from Fig. 10 with $\tau = 5\%, 50\%, 95\%$.

Conjecture 6.1. *There is a threshold variance σ_0 such that if $\sigma > \sigma_0$, then the energy of the kth mode satisfies $|E_k(t) - E_k(0)| \ll 1$ for $k < k_0$ for a sufficiently long time.*

It would definitely be a significant result if this statement could be proven. Our immediate future work would be to consider, e.g., how σ_0 would scale with N and how the localization phenomenon would happen in the limit $N \to \infty$. Our preliminary results also indicate that the coefficients of the coupling terms in the two-mode approximation (25), i.e., $\widetilde{A}$ and $\widetilde{B}$, decrease with increasing N for the same variability tolerance. This may mean that the larger the number of particles N, the easier the system experiences energy localization due to disorder.

We also have studied the effect of variability on the chaotic behavior of the system by calculating the maximum Lyapunov exponent for several realizations for the same variability percentage. We have found that it is more likely to observe chaotic trajectories as we increase the number of particles N for 5% and 50% tolerance. However, at 95% tolerance, the percentage of chaotic trajectories grows for $N = 4, 8, 16$ but slightly declines for $N = 32$. Moreover, we have also investigated the connection between energy localization and the chaotic features of its trajectory. We have found that when the trajectory is regular, either energy recurrence or energy localization occurs. On the other hand, a chaotic trajectory leads to energy thermalization. As our present study on chaotic trajectories in the disordered system is rather limited to small numbers of particles, considering large values of N is of interest, especially in the thermodynamics limit.

7. Acknowledgement

We thank the two reviewers for their comments and feedback, which significantly improved the manuscript. Z. is supported by the Ministry of Education, Culture, Research, and Technology of Indonesia through a PhD scholarship (BPPLN). H.S. acknowledges support from Khalifa University through a Faculty Start-Up Grant (No. 8474000351/FSU-2021-011) and a Competitive Internal Research Awards Grant (No. 8474000413/CIRA-2021-065). The authors acknowledge the use of the High-Performance Computing Facility (Ceres) and its associated support services at the University of Essex in completing this work.

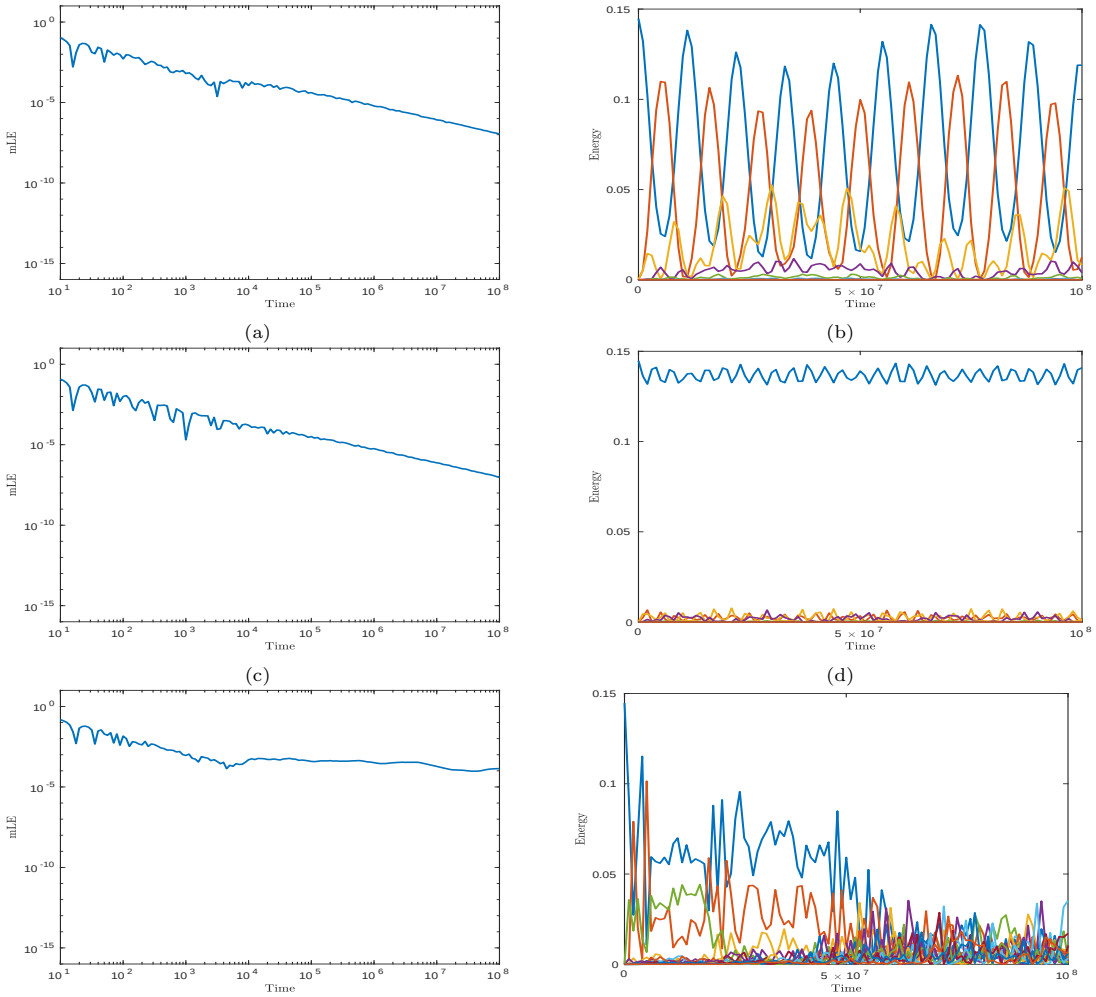

Figure 12: The maximum Lyapunov exponent (mLE) and its corresponding normal-mode energy for $N = 16$ and tolerance $\tau = 5\%$ in panels (a)-(b), $\tau = 50\%$ in panels (c)-(d), and $\tau = 95\%$ in panels (e)-(f) .

References

[1] E. Fermi, J. Pasta, S. Ulam, Los Alamos report LA-1940, Fermi, Collected Papers 2 (1955) 977–988.

[2] J. L. Tuck, M. T. Menzel, The superperiod of the nonlinear weighted string (FPU) problem, Advances in Mathematics 9 (3) (1972) 399–407.

[3] S. D. Pace, D. K. Campbell, Behavior and breakdown of higher-order Fermi-Pasta-Ulam-Tsingou recurrences, Chaos: An Interdisciplinary Journal of Nonlinear Science 29 (2) (2019) 23132.

[4] H. Nelson, M. A. Porter, B. Choubey, Variability in Fermi-Pasta-Ulam-Tsingou arrays can prevent recurrences, Phys. Rev. E 98 (6) (2018) 62210. doi:10.1103/PhysRevE.98.062210. URL https://link.aps.org/doi/10.1103/PhysRevE.98.062210

[5] K. R. Allen, J. Ford, Lattice thermal conductivity for a one-dimensional, harmonic, isotopically disordered crystal, Physical Review 176 (3) (1968) 1046.

[6] P. W. Anderson, Absence of diffusion in certain random lattices, Physical Review 109 (5) (1958) 1492.

[7] H. Matsuda, K. Ishii, Localization of normal modes and energy transport in the disordered harmonic chain, Progress of Theoretical Physics Supplement 45 (1970) 56–86.

[8] B. Li, H. Zhao, B. Hu, Can disorder induce a finite thermal conductivity in 1d lattices?, Physical Review Letters 86 (1) (2001) 63.

[9] A. Dhar, K. Saito, Heat conduction in the disordered Fermi-Pasta-Ulam chain, Physical Review E—Statistical, Nonlinear, and Soft Matter Physics 78 (6) (2008) 061136.

[10] J. Zhu, Y. Liu, D. He, Effects of interplay between disorder and anharmonicity on heat conduction, Physical Review E 103 (6) (2021) 062121.

[11] S. Liu, X. Xu, R. Xie, G. Zhang, B. Li, Anomalous heat conduction and anomalous diffusion in low dimensional nanoscale systems, The European Physical Journal B 85 (2012) 1–20.

[12] H. Christodoulidi, C. Efthymiopoulos, T. Bountis, Energy localization on q-tori, long-term stability, and the interpretation of Fermi-Pasta-Ulam recurrences, Physical Review E 81 (1) (2010) 016210.

[13] H. Christodoulidi, C. Efthymiopoulos, Low-dimensional q-tori in FPU lattices: Dynamics and localization properties, Physica D: Nonlinear Phenomena 261 (2013) 92–113.

[14] A. Ponno, H. Christodoulidi, C. Skokos, S. Flach, The two-stage dynamics in the Fermi-Pasta-Ulam problem: From regular to diffusive behavior, Chaos: An Interdisciplinary Journal of Nonlinear Science 21 (4) (2011) 043127. arXiv:1107.2626, doi:10.1063/1.3658620.

[15] B. Rink, Proof of nishida's conjecture on anharmonic lattices, Communications in mathematical physics 261 (3) (2006) 613–627.

[16] A. Henrici, T. Kappeler, Results on normal forms for FPU chains, Communications in mathematical physics 278 (1) (2008) 145–177.

[17] T. Kappeler, A. Henrici, Resonant normal form for even periodic FPU chains, Journal of the European Mathematical Society 11 (5) (2009) 1025–1056.

[18] N. J. Zabusky, M. D. Kruskal, Interaction of" solitons" in a collisionless plasma and the recurrence of initial states, Physical Review Letters 15 (6) (1965) 240.

[19] A. Ponno, Soliton theory and the Fermi-Pasta-Ulam problem in the thermodynamic limit, Europhysics Letters 64 (5) (2003) 606.

[20] D. Bambusi, A. Ponno, On metastability in fpu, Communications in mathematical physics 264 (2006) 539–561.

[21] M. Gallone, A. Ponno, B. Rink, Korteweg–de Vries and Fermi–Pasta–Ulam–Tsingou: asymptotic integrability of quasi unidirectional waves, Journal of Physics A: Mathematical and Theoretical 54 (30) (2021) 305701.

[22] M. Gallone, M. Marian, A. Ponno, S. Ruffo, Burgers turbulence in the Fermi-Pasta-Ulam-Tsingou chain, Physical Review Letters 129 (11) (2022) 114101.

[23] W. Ferguson Jr, H. Flaschka, D. McLaughlin, Nonlinear normal modes for the Toda chain, Journal of computational physics 45 (2) (1982) 157–209.

[24] D. Bambusi, A. Maspero, Birkhoff coordinates for the Toda lattice in the limit of infinitely many particles with an application to fpu, Journal of Functional Analysis 270 (5) (2016) 1818–1887.

[25] G. Benettin, G. Orsatti, A. Ponno, On the role of the integrable Toda model in one-dimensional molecular dynamics, Journal of Statistical Physics 190 (8) (2023) 131.

[26] T. Grava, A. Maspero, G. Mazzuca, A. Ponno, Adiabatic invariants for the FPUT and Toda chain in the thermodynamic limit, Communications in Mathematical Physics 380 (2) (2020) 811–851.

[27] F. J. Dyson, The dynamics of a disordered linear chain, Physical Review 92 (6) (1953) 1331.

[28] D. Kulkarni, D. Schmidt, S.-K. Tsui, Eigenvalues of tridiagonal pseudo-Toeplitz matrices, Linear Algebra and its Applications 297 (1999) 63–80.

[29] M. Syafwan, H. Susanto, S. M. Cox, Discrete solitons in electromechanical resonators, Physical Review E 81 (2) (2010) 26207.

[30] J. Pickton, H. Susanto, Integrability of PT-symmetric dimers, Physical Review A 88 (6) (2013) 63840.

[31] G. Benettin, A. Ponno, Time-scales to equipartition in the fermi–pasta–ulam problem: finite-size effects and thermodynamic limit, Journal of Statistical Physics 144 (2011) 793–812.

[32] K. A. Reiss, D. K. Campbell, The metastable state of Fermi–Pasta–Ulam–Tsingou models, Entropy 25 (2) (2023) 300.

[33] G. Benettin, R. Livi, A. Ponno, The Fermi-Pasta-Ulam problem: scaling laws vs. initial conditions, Journal of Statistical Physics 135 (2009) 873–893.

[34] G. Benettin, A. Ponno, FPU model and Toda model: a survey, a view, in: INdAM Workshop The Legacy of Carlo Cercignani: from Kinetic Theory to Turbulence Modeling, Springer, 2021, pp. 21–44.

[35] G. Benettin, L. Galgani, A. Giorgilli, J.-M. Strelcyn, Lyapunov characteristic exponents for smooth dynamical systems and for Hamiltonian systems; a method for computing all of them. Part 1: Theory, Meccanica 15 (1) (1980) 9–20.

[36] C. Skokos, The Lyapunov characteristic exponents and their computation, in: Dynamics of Small Solar System Bodies and Exoplanets, Springer, 2010, pp. 63–135.

[37] C. Skokos, E. Gerlach, Numerical integration of variational equations, Physical Review E 82 (3) (2010) 36704.

[38] H. Yoshida, Construction of higher order symplectic integrators, Physics Letters A 150 (5-7) (1990) 262–268.

[39] G. P. Drago, S. Ridella, Some more observations on the superperiod of the non-linear FPU system, Physics Letters A 122 (8) (1987) 407–412.

[40] D. S. Sholl, B. I. Henry, Recurrence times in cubic and quartic Fermi-Pasta-Ulam chains: A shifted-frequency perturbation treatment, Physical Review A 44 (10) (1991) 6364.